J Mater Sci (2006) 41:7989–8000
DOI 10.1007/s10853-006-0864-3

Lattice Boltzmann method based computation of the permeability of the orthogonal plain-weave fabric preforms

M. Grujicic · K.M. Chittajallu · Shawn Walsh

Received: 9 July 2005 / Accepted: 7 November 2005 / Published online: 22 September 2006

Abstract Changes in the permeability tensor of fabric preforms caused by various modes of fabric distortion and fabric-layers shifting and compacting is one of the key factors controlling resin flow during the infiltration stage of the common polymer-matrix composite liquid-molding processes. While direct measurements of the fabric permeability tensor generally yield the most reliable results, a large number of fabric architectures used and numerous deformation and layers rearrangement modes necessitates the development and the use of computational models for prediction of the preform permeability tensor. The Lattice Boltzmann method is used in the present work to study the effect of the mold walls, the compaction pressure, the fabric-tows shearing and the fabric-layers shifting on the permeability tensor of preforms based on orthogonal balanced plain-weave fabrics. The model predictions are compared with their respective experimental counterparts available in the literature and a reasonably good agreement is found between the corresponding sets of results.

Nomenclature

f Particle distribution function
f_f Fiber volume fraction
h Fabric thickness (m)
ϕ Relative dimensionless shift of the adjacent fabric layers
K Permeability tensor of the fabric (m^2)
L In-plane quarter cell dimension (m)
p Pressure (Pa)
α Shear angle (deg.)
r_f Fiber radius (m)
s Relative shift of the adjacent fabric layers (m)
e Particle velocity component
ρ Fluid point density (particles/lattice point)
Ω Collision operator
t Time (s)
τ Time relaxation parameter
t_i Velocity component weighting factor
u Fluid nodal velocity (lattice parameters/time increment)
v Fluid kinematic viscosity (m^2/s)
x Nodal position vector

Subscripts

bot Quantity associated with the bottom surface of the fabric
top Quantity associated with the top surface of the fabric

Superscripts

B Quantity associated with the bottom channel
eq Equilibrium quantity
F Quantity associated with the fabric
T Quantity associated with the top channel

M. Grujicic (✉) · K.M. Chittajallu
Department of Mechanical Engineering,
Clemson University, 241 Engineering Innovation Building,
Clemson, SC 29634-0921, USA
e-mail: mica.grujicic@ces.clemson.edu

S. Walsh
Army Research Laboratory—WMRD AMSRL-WM-MD,
Proving Ground, Aberdeen, MD 21005-5069, USA

Introduction

Over the last two decades, major advances in the resin-injection technologies have enabled the processing of

high-performance polymer-matrix composites expand from their aerospace roots to diverse military and civil applications. At the same time, the processing science has become an integral part of the composite-manufacturing technology so that empiricism and semi-empiricism have given way to a greater use of computer modeling and simulations of the fabrication processes. Among the modern polymer-matrix composite manufacturing techniques, liquid-molding processes such as Resin Transfer Molding (RTM), Vacuum Assisted Resin Transfer Molding (VARTM) and Structural Reaction Injection Molding (SRIM) have a prominent place. A detailed review of the major liquid molding processes can be found in the recent work of Lee [1]. One common feature to all these composite fabrication processes is the use of low-pressure infiltration of the porous fabric preforms with a viscous fluid (resin). Conformation of the fabric preforms to the ridges and recesses in the mold and the applied pressure can induce significant distortions and deformations in the fabric as well as give rise to shifting of the individual fabric layers and, in turn, cause significant change in local permeability of the preform. Since the infiltrating fluid follows the path of least resistance, local changes in the fabric permeability can have a great influence on the mold filling process affecting the filling time, the filling completeness and the formation of pores and dry spots. Hence, a better understanding of the changes in fabric permeability caused by various local distortions, shearing and shifting of its tows is critical for proper design of the liquid molding fabrication processes.

In simple terms, permeability can be defined as a (tensorial) quantity which relates the local average *superficial* velocity vector of the fluid with the associated pressure gradient. In polymer-matrix composite liquid-molding processes such as the RTM and the VARTM, the porous medium consists of woven- or weaved-fabric preforms placed in the mold and the fluid flow of interest involves preform infiltration with resin. Complete infiltration of the preform with resin is critical for obtaining high-integrity and high-quality composite structures. The knowledge of the preform permeability and its changes due to fabric bending, shearing, compression, shifting, etc. is crucial in the design of a composite fabrication process (e.g., in the design of the tool plate, or for placement of the resin injection ports).

While direct experimental measurements of the fabric permeability is generally considered as most accurate and most reliable, it suffers from a number of limitations such as: (a) experimental set-ups can be elaborate and the measurements very time consuming; (b) experimental measurements have to be done for each new architecture and/or deformation state of the fiber preform; and (c) experiments involve measurements of the (macro) preform length-scale flow parameters (e.g., the flow length or the shape and the size of a flow front) are used to infer a (meso) fabric/fiber length-scale parameter (the permeability tensor). In more complex preform architectures, this procedure is a formidable task and can be accompanied with substantial experimental and data reduction errors. Consequently, development of the computational models for prediction of the preform permeability tensor to complement experimental measurements has become a standard practice.

For the computational modeling approach to be successful in predicting permeability of the fabric preforms, it must include, in a correct way, both the actual architecture of the fabric and the basic physics of the flow through it. A schematic of the relatively simple orthogonal plain-weave one-layer fabric architecture is shown in Fig. 1. As seen in Fig. 1, the fabric consists of orthogonal (warp and weft) yarns, which are woven together to form an interconnected network. Each yarn, on the other hand, represents a long continuous length of interlocked fibers, normally grouped into bundles (threads) twisted together to form the final yarn. In addition, the fabric involves a network of empty pores and channels. When a fabric like the one shown in Fig. 1 is being infiltrated, the resin flows

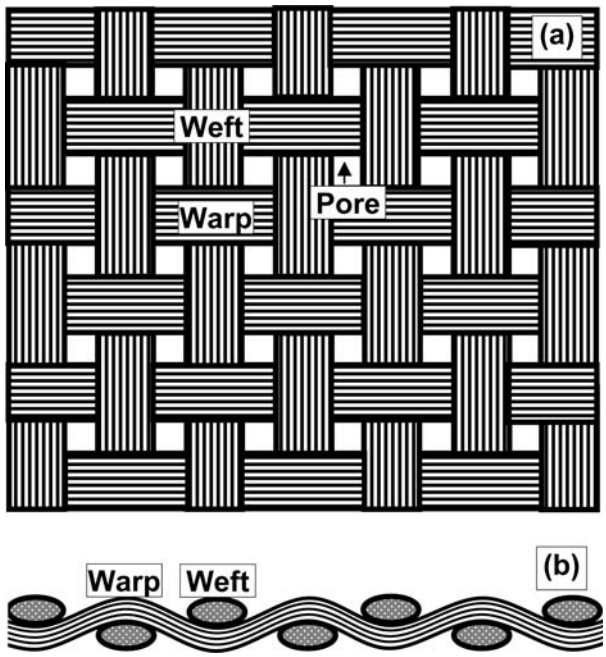

Fig. 1 A schematic of (**a**) the top view and (**b**) the edge view of a one-layer orthogonal plain-weave fabric preform

mainly through the pores and the channels. However, since the fabric tows are porous (pores and channel on a finer length scale exist between the fibers in tows), the resin also flows within the yarn. Thus, when predicting the effective permeability of a fabric, the computational model should account for both components of the resin flow.

Prediction of the permeability of porous medium has been the subject of intense research for at least last two decades. Due to space limitations in this paper, it is not possible to discuss all the models proposed over this period of time. Nevertheless, one can attempt to classify the models. One such classification involves the following main types of models for permeability prediction in the porous media: (a) the phenomenological models based on the use of well-established physical concepts such as the capillary flow (e.g., [2, 3]) or the lubrication flow (e.g., [4]). These models generally perform well within isotropic porous media with a simple architecture; (b) the numerical models which are based on numerical solutions of the governing differential equations. These models generally attempt to realistically represent the architecture of the fiber preform but, due to limitations in the computer speed and the memory size, are ultimately forced to the introduction of a number of major simplifications (e.g., [5, 6]); and (c) the models which are based on a balance between the fabric-architecture and the flow physics simplifications, enabling physically based predictions of the preform permeability within reasonably realistic fabric architectures [7].

Over the last decade, the Lattice Boltzmann method has become a respectable alternative to the classical Navier–Stokes equations based computations of various fluid flow phenomena. In particular, the lattice Boltzmann method has been found to offer computational advantage in the analyses of fluid flow in media with a complex geometry [8, 9], in multi-length-scale porous media [10], moving boundary multi-phase flow [11]. Since, in general, fabric preforms act as a porous media with complex multi-length-scale architectures, and the dynamics of their filling during the resin injection stage of the RTM and VARTM processes, the Lattice Boltzmann method has been used in the present work to compute the permeability components of fabric preforms under different modes of deformation. The permeability components are next assembled into a permeability tensor.

The organization of the paper is as follows: A brief overview of the fabric architectures and the Lattice Boltzmann method is presented in ''Computional procedure'' section. The application of the Lattice Boltzmann method to revealing the role of various fabric distortion and layers-compaction and shifting phenomena is presented and discussed in ''Results and discussion'' section. The main conclusions resulted from the present work are summarized in ''Conclusions'' section.

Computational procedure

Fabric architecture

Single-layer fabrics

In this work, only (un-sheared and sheared) balanced orthogonal plain-weave fabric is considered. Due to the in-plane periodicity, the fabric architecture can be represented using a unit cell. The entire orthogonal plain-weave fabric can then be obtained by repeating the unit cell in the in-plane (x- and y-) directions. A schematic of one quarter of a plain-weave unit cell with the appropriate denotation for the system dimensions are shown in Fig. 2. In a typical plain-weave fabric, the fabric thickness (h) to the quarter cell in-plane dimension (L) ratio, h/L, is small (0.01–0.1), while the tow cross-section is nearly elliptical in shape with a large (width-to-height) aspect ratio (five or larger). The geometry of the tows within the cell can be described using various mathematical expressions (e.g., [12]) for the top, $z_{\text{top}}(x,y)$, and the bottom, $z_{\text{bot}}(x,y)$, surfaces of the fabric, respectively. In the present work, the following sinusoidal functions originally proposed by Ito and Chou [13] are used:

$$z_{\text{top}}(x,y) = \frac{h}{2}\left(\sin\frac{2\pi}{L}x + \sin\frac{2\pi}{L}y\right) \tag{1}$$

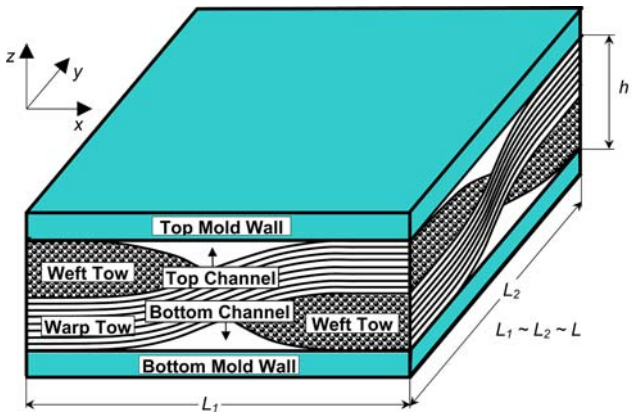

Fig. 2 Schematic of one quarter of the unit cell for a one-layer balanced orthogonal plain-weave fabric

$$z_{\text{bot}}(x,y) = -\frac{h}{2}\left(\sin\frac{2\pi}{L}x + \sin\frac{2\pi}{L}y\right) \quad (2)$$

Since the fiber tows have typically a near elliptical cross-section, Eqs. (1) and (2) only approximate the actual tow cross-section shape. Nevertheless, they are used in the present work since they greatly simplify permeability calculations in the distorted fabric and are generally considered as a good approximation for the actual tow cross-section shape.

A simple examination of Fig. 2 shows that within a single-layer orthogonal plain-weave fabric unit cell, one can identify three distinct domains:

The top channel, Region $T : z_{\text{top}} < z < \frac{h}{2}$

The fabric, Region $F : z_{\text{bot}} < z < z_{\text{top}}$

The bottom channel, Region $B : -\frac{h}{2} < z < z_{\text{bot}}$

Regions T and B contain only the resin, while region F can generally contain both the fiber tows and the resin. The resin flow through a unit cell is analyzed in the present work by considering only the flow within the top and the bottom channels. In our previous work [7], it was shown that the resin flow within the fabric has a minor contribution to the overall permeability of the perform.

Multi-layer fabrics

In typical RTM and VARTM processes, the preforms may contain several fabric layers. In such multi-layer preforms, nesting and compaction can generally have a significant effect and must be included when predicting preform permeability. Numerous experiments (e.g., [14, 15]) confirmed that permeability varies with the number of layers. A schematic of two types of two-layer plain-weave fabric preforms analyzed in the present work is given in Fig. 3(a) and (b). The two types are generally referred to as ''in-phase'' and ''out-of-phase'' fabric architectures or laminates. The mathematical expressions for the top and the bottom surfaces in each preform layer can be readily defined using Eqs. (1) and (2).

Sheared fabrics

As pointed out earlier, when the fabric preform is forced to conform to the ridges and recesses of a mold,

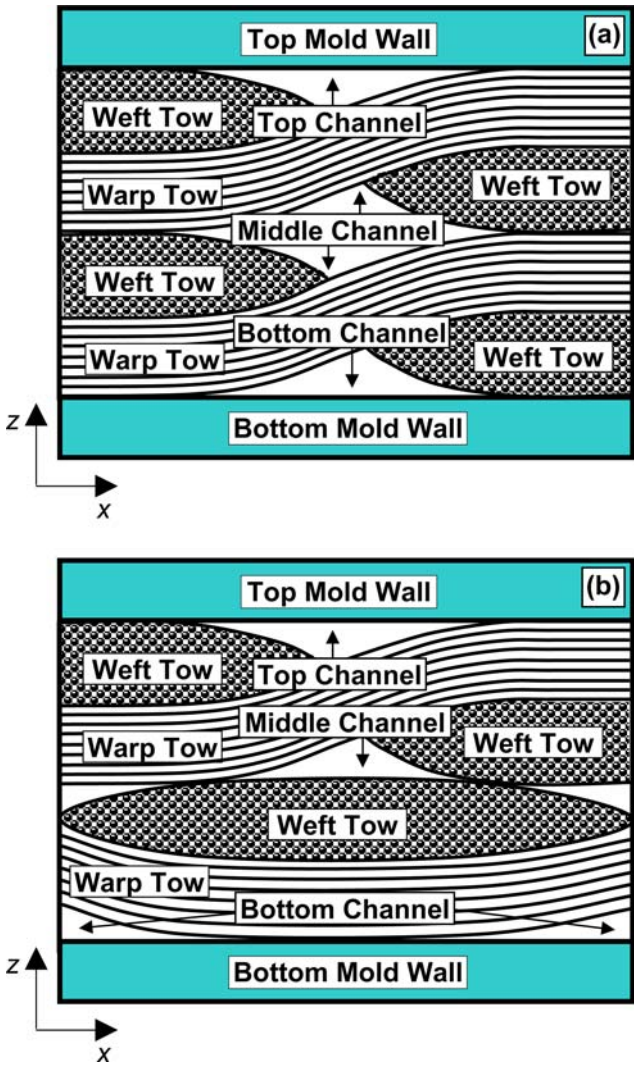

Fig. 3 $x - z$ section of a quarter of the unit cell for: (**a**) an in-phase; and (**b**) an out-of-phase two-layer orthogonal plain-weave fabric

it may locally undergo shear deformation. Such deformation can significantly affect local permeability of the preform. As shown in Fig. 4, when a balanced square-cell plain-weave fabric is sheared, the unit cell size increases and to make the calculations of preform permeability manageable, the shear angle $\alpha = \tan^{-1}(m/n)$ is generally allowed to take only the values corresponding to relatively small integers m and n.

Compacted fabrics

When the fabric is subjected to compression during mold closing in the RTM process or during evacuation of the vacuum bag in the VARTM process, it undergoes a number of changes such as: the cross-section of the fiber tow flattens, the pores and gaps between the

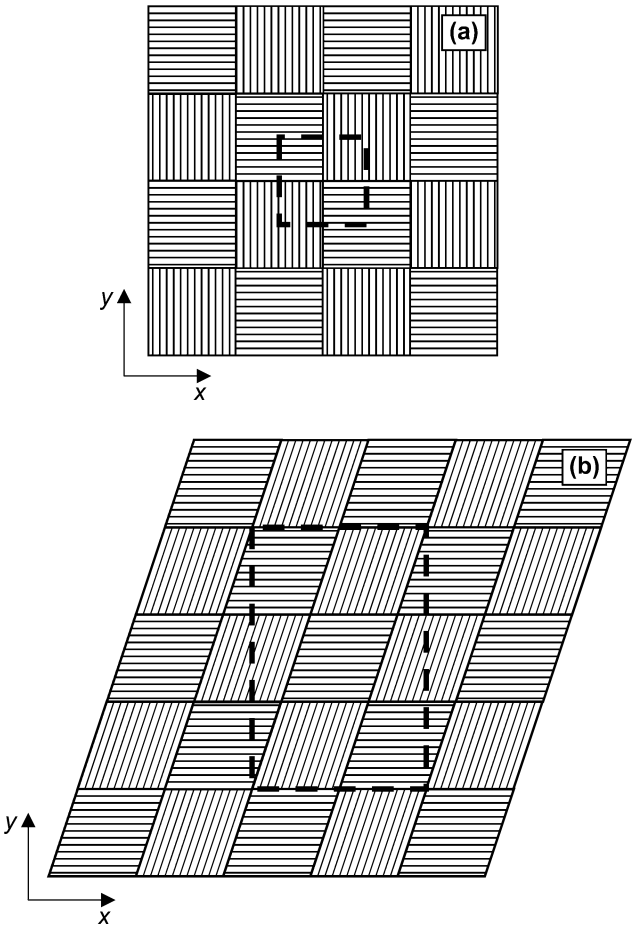

Fig. 4 Effect of fabric shearing on the size of the quarter unit cell (denoted using heavy dashed lines) in balanced plain-weave fabric architectures: (**a**) un-sheared fabric; (**b**) fabric sheared by an angle $\alpha = \tan^{-1}(1/3)$ in the x-direction

fibers inside tows as well as between individual tows are reduced, the tows undergo elastic deformation, inter-layers shifting (nesting), etc. A typical compression-pressure versus preform thickness curve for a woven fabric is depicted in Fig. 5 [16]. The curve shown in Fig. 5 has three distinct parts: two linear and one non-linear. In the low-pressure linear and the non-linear portions of the pressure versus thickness curve, preform compaction is dominated by a reduction of the pore and the gap sizes between the fibers in tows. In the high-pressure linear region of the pressure versus thickness curve, on the other hand, preform compaction involves mainly tow bending and nesting as well as fiber compression. Typical liquid molding processes such as RTM or VARTM involve pressures which correspond to the high-pressure linear pressures versus thickness region. Hence, the effect of fabric compaction on permeability of the fabric preform associated with the high-pressure linear compaction regime is investigated in this section.

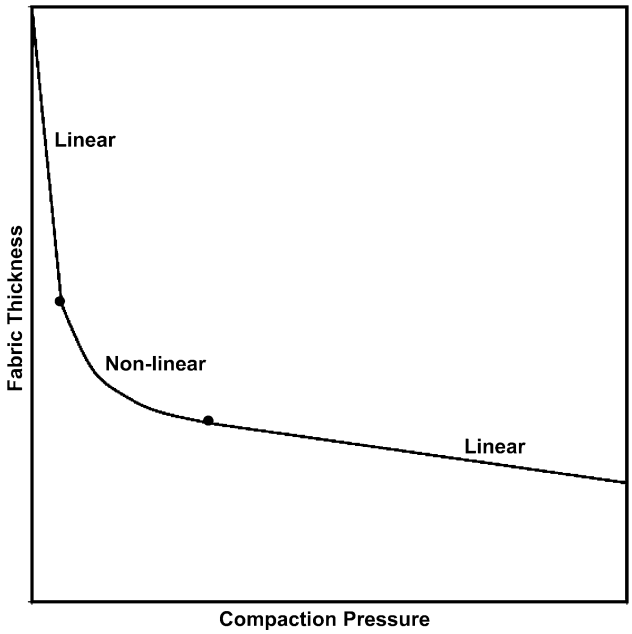

Fig. 5 A typical compaction-pressure versus preform-thickness curve for a plain-weave fabric architecture

To quantify the effect of preform compaction (in the high-pressure linear region) on permeability of the balanced orthogonal plain-weave fabric, the beam-bending based micro-mechanical model developed in a series of papers by Chen and Chou [17–19] is utilized in the present work. The model of Chen and Chou [17–19] is based on a number of well-justified assumptions such as: (a) the fabric is considered to extend indefinitely in the $x - y$ plane and, hence, can be represented using the unit cells such as the one shown in Fig. 2; (b) tows in the fabric are treated as a transversely isotropic solid material; (c) the fabric is subjected to the compaction pressure only in the through-the-thickness direction, and can freely adjust its shape in the $x - y$ plane. This assumption is less justifiable in the regions of the fabric which are in direct contact with the mold where friction can impose some lateral constraint to the fabric. No attempt was made in the present work to quantify this effect; (d) since the compaction analyzed corresponds to the high-pressure linear region, no voids or gaps are assumed to exist between the fibers in tows or between the tows; (e) during fabric compaction, the cross-section area of the tows is assumed to remain unchanged but the shape of the cross-section undergoes a change; and (f) as compaction proceeds, the deformation of the tows leads to an increase in the effective volume fraction of the fibers in the fabric and, in the limit of complete compaction of the tows, the volume fraction of the fibers in the fabric becomes equal to that in the individual tows.

In order to derive a relationship between the reduction in the fabric thickness, the effective volume fraction of the fibers and various distributions and magnitudes of the applied compaction pressure, Chen and Chou [17–19] applied a simple procedure from the solid-mechanics beam theory. Toward that end, the one-quarter unit cell shown in Fig. 2 is first simplified by replacing the two warp and the two weft tows with four beams. Next based on the symmetry of the simplified model, it is shown that the problem can be further simplified using a single beam and the appropriate distribution of the applied and contacting pressures, Fig. 6. The model of Chen and Chou [17–19] is utilized in the present work to compute the effect of the compaction pressure on the channel heights ($h^{T}(x,y)$ and $h^{B}(x,y)$) and on the fabric thickness, $h^{F}(x,y)$ fields. These fields are used to quantify the effect of fabric compaction on the effective permeability of a one-layer orthogonal plain-weave fabric.

Nested fabrics

As mentioned earlier, shifting of fabric layers followed by their more compact packing (the phenomenon generally referred to as layers "*nesting*") can have a major effect on the effective fiber density in the preform and, hence, on permeability of the preform. Nesting of the fabric layers can particularly take place under high applied pressures which are sufficient to overcome inter-tow friction. The thickness reduction in balanced orthogonal plain-weave fabrics whose geometry is represented by Eqs. (1) and (2), due to layers nesting has been analyzed by Ito and Chou [13] who derived the following relation for the fabric thickness reduction caused by nesting:

$$\Delta h^{\text{nesting}} = h\begin{cases} 2-\cos\frac{\phi_x}{2}-\cos\frac{\phi_y}{2}, & |\phi_x|\le\frac{\pi}{2},|\phi_y|\le\frac{\pi}{2} \\ 2-\sin\frac{|\phi_x|}{2}-\cos\frac{\phi_y}{2}, & \frac{\pi}{2}\le|\phi_x|\le\pi,|\phi_y|\le\frac{\pi}{2} \\ 2-\cos\frac{\phi_x}{2}-\sin\frac{|\phi_y|}{2}, & |\phi_x|\le\frac{\pi}{2},\frac{\pi}{2}\le|\phi_y|\le\pi \\ 2-\sin\frac{|\phi_x|}{2}-\sin\frac{|\phi_y|}{2}, & \frac{\pi}{2}\le|\phi_x|\le\pi,\frac{\pi}{2}\le|\phi_y|\le\pi \end{cases} \tag{3}$$

where $\phi_x = \frac{2\pi}{L}s_x$ and $\phi_y = \frac{2\pi}{L}s_y$ are dimensionless while s_x and s_y are the dimensional relative shifts of the adjacent layers in the x- and y-directions, respectively.

Two non-nesting cases associated with zero nesting, reduction in the fabric thickness can be identified: (a) $\phi_x = \phi_y = 0$ which corresponds to the iso-phase laminate case and (b) $\phi_x = \phi_y = \pm\pi/2$ corresponding to the out-of-phase laminate case.

The relations given in Eq. (3) are used in the present work to examine the effect of layers nesting on fabric permeability. While, in general, fabric compaction during the high-pressure linear compaction stage can involve both elastic distortions (tow bending) and layers nesting, the two modes of fabric compaction are generally considered as decoupled and can be considered separately.

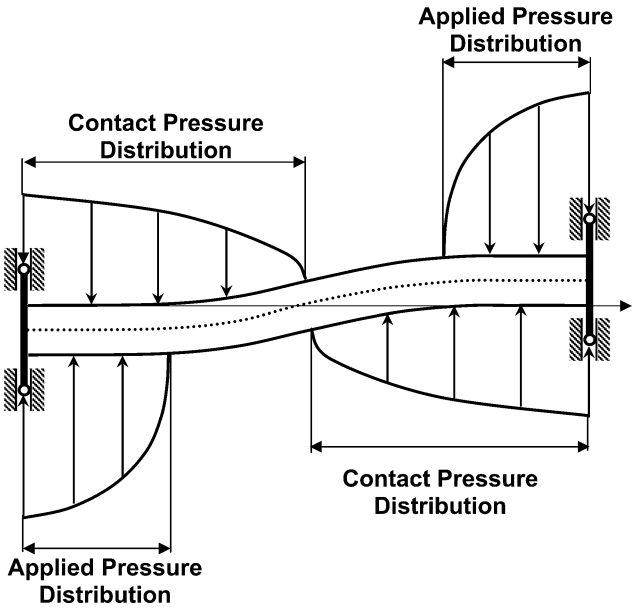

Fig. 6 A schematic of the pressure distribution on a curved beam used in the calculation of permeability of un-sheared one-layer orthogonal plain-weave fabrics

The Lattice Boltzmann method

As stated earlier, the computation of the fabric-preform permeability tensor is carried out in the present work using the Lattice Boltzmann method. Within this method, the (continuum) physical space is replaced with a large number (typically 10^6–10^7) of discrete points (nodes). When such nodes do not reside within a solid (e.g., the points located outside the mold walls or reinforcing fibers), they are assumed to be populated with "fluid" particles. Particles residing on a node are allowed to have only one of a finite number of velocities (typically the pores with a direction toward the nearest and the next nearest neighbor nodes). For example, in the D3Q19 lattice used in the present

work, Fig. 7, any particle residing at node denoted as 0 can have either a zero velocity (be stationary) or have a velocity with a direction toward the nearest neighbor nodes (nodes 1, 3, 5, 7, 9, 18) and toward the next nearest neighbor nodes (nodes 2, 4, 6, 8, 10–17). The magnitude of the velocity is the same for all particles and it is equal to a ratio of the lattice constant and the time increment. Within the Lattice Boltzmann method, then, one computes the temporal and spatial evolutions of a distribution functions for such particles. Macroscopic fluid quantities such as the point density $\rho(\mathbf{x},t)$, and the velocity $u(\mathbf{x},t)$ (where $\mathbf{x}$ is the node position vector and t the time), can then be computed as simple moment sums of these particle distribution functions as:

$$\rho(\mathbf{x},t) = \sum_{i=1}^{n} f_i(\mathbf{x},t) \tag{4}$$

and

$$u(\mathbf{x},t) = \frac{\sum_{i=1}^{n} f_i(\mathbf{x},t)\mathbf{e}_i}{\rho(\mathbf{x},t)} \tag{5}$$

where $f_i(\mathbf{x},t)$ is the particle distribution function, i is the velocity component, n is the total number of velocity components per node (1 + the number of nearest neighbors (6) + the number of next nearest neighbors (12) = 19, in the case of the D3Q19 lattice).

The evolution of the particle distribution function $f_i(\mathbf{x},t)$ is governed by the Lattice Boltzmann equation as:

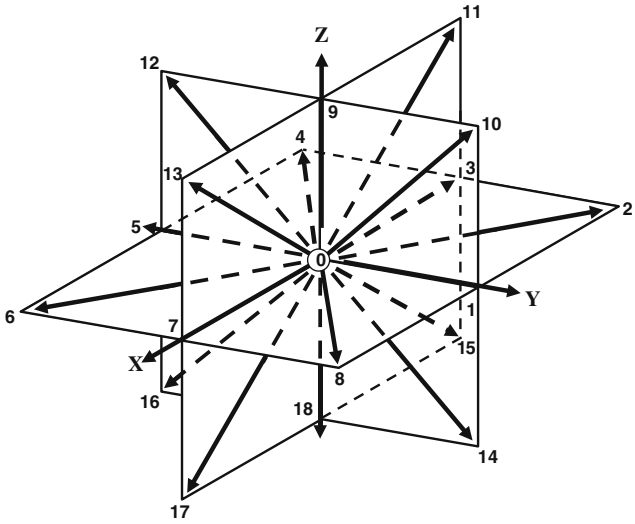

Fig. 7 The D3Q19 lattice consisting of 19 particle velocity vectors including the zero-magnitude velocity vector for stationary particles denoted as "O"

$$f_i(\mathbf{x}+\mathbf{e}_i, t+1) = f_i(\mathbf{x},t) + \Omega_i(\mathbf{x},t) \tag{6}$$

where the time increment is set explicitly to 1.

The collision operator, $\Omega_i(\mathbf{x},t)$ on the right hand side of Eq. (6), represents the rate of change of the particle distribution function due to particle collisions at the nodes. Following Bhatnager et al. [20], the collision operator is greatly simplified (the so-called BGK simplification) through the use of a single time relaxation parameter τ as:

$$\Omega_i(\mathbf{x},t) = -\frac{1}{\tau}\left(f_i(\mathbf{x},t) - f_i^{\mathrm{eq}}(\mathbf{x},t)\right) \tag{7}$$

where $f_i^{\mathrm{eq}}(\mathbf{x},t)$ is the equilibrium particle distribution function at the node with a position vector, $\mathbf{x}$, at time, t, while τ controls the rate at which the particle distribution function approaches its equilibrium value.

The equilibrium particle distribution is represented by relations:

$$f_0^{\mathrm{eq}}(\mathbf{x},t) = \frac{\rho(\mathbf{x})}{3}\left[1 - \frac{3}{2}|\mathbf{u}(\mathbf{x},t)|^2\right] \tag{8}$$

and

$$f_i^{\mathrm{eq}}(\mathbf{x},t) = t_i\rho(\mathbf{x}) \times \left[1 + 3\mathbf{e}_i\cdot\mathbf{u}(\mathbf{x},t) + \frac{3}{2}\left(3\mathbf{e}_i\mathbf{e}_i : \mathbf{u}(\mathbf{x},t)\mathbf{u}(\mathbf{x},t) - |\mathbf{u}(\mathbf{x},t)|^2\right)\right] \quad \text{for } i \neq 0; \tag{9}$$

and for the D3Q19 lattice, $t_i = 1/6$ for the velocities along the Cartesian axes (the ones with the direction toward the nearest neighbor nodes) and $t_i = 1/36$ for the remaining velocities. Chen et al. [21] showed that the formulation of the Lattice Boltzmann method presented above yields a velocity field which is a solution to the Navier–Stokes equation with the kinematic viscosity equal to:

$$v = \frac{\tau - 0.5}{3} \tag{10}$$

It should be noted that the equilibrium particle-velocity distribution function defined by Eqs. (8) and (9) are derived under the condition that the imposed (average) density/velocity are consistent with the ones obtained using Eqs. (4) and (5).

Computer program

The computation of the fabric permeability tensor has been carried out using H. W. Stockman's Lattice Boltzmann JB_PH code [22], a program for modeling

multi-component flow and dispersion. Due to the use of an optimization scheme and the BGK simplification of the Lattice Boltzmann method, the code is quite fast even on a single-CPU computer so that complex solids geometries containing millions of nodes can be modeled. Accuracy of the code has been validated using four benchmark problems: (a) permeability of a simple cubic array of spheres; (b) Taylor-Aris dispersion between infinite plates; (c) dispersion in a duct; and (d) dispersion in a simple cubic array of spheres.

Results and discussion

Un-sheared single-layer plain-weave fabric preforms

The Lattice Boltzmann method briefly overviewed in "The Lattice Boltzmann method" section is used in this section to analyze the velocity distributions within the un-sheared single-layer balanced orthogonal plain-weave quarter unit cell. It should be pointed out that due to the symmetry of the unit cell with respect to the $z = 0$ mid-plane, the velocity distributions within the top and the bottom resin channels are expected to be identical and, hence, no transverse flow of the resin through the fabric preform is expected. Also, it should be noted that due to the symmetry of the fabric geometry with respect to the quarter unit-cell boundaries normal to the y-direction, a zero fluid-flow velocity is expected across these boundaries.

The variations of the top- and bottom-channel heights and of the fabric thickness in the $x - y$ plane within a quarter unit cell, used as input in the present analysis, are shown in Fig. 8(a) and (b), respectively. The variations of the x-component resin velocity within the resin channels of a quarter unit cell over the $x - y$ planes corresponding to $y = 0$ and $y = L/2$ are for the fixed imposed pressure gradient $dP/dx = -F_x\rho = 1.0 \times 10^7$ Pa/m in the x-direction (F_x is the x-component of the body force) are shown in Fig. 9(a) and (b). The results displayed in Fig. 9(a) and (b) show that the velocity distribution is symmetric about the $z = 0$ mid-plane. In addition, a comparison of the results shown in Fig. 9(a) and (b) with the ones shown in Fig. 8(a) and (b) reveals that the magnitude of the x-component of the resin velocity at a given $x - y$ location correlates inversely with the local height of the resin channel in order to satisfy the continuity equation. It should be noted that in order to improve clarity, the dimension of the quarter unit cell in the z-direction is magnified ten times in Fig. 9(a) and (b).

Effect of the number of layers in un-sheared plain-weave fabric preforms

The Lattice Boltzmann method is used in the present section to predict permeability of the balanced un-sheared single- and multi-layer orthogonal plain-weave fabric architectures. In all the calculations carried out in this section, as well as in the calculations carried out in the previous section, the following unit cell parameter and one-layer fabric thickness values are used: $L_1 = L_2 = L = 0.01$ m and $h = 0.001$ m.

To determine the permeability tensor, the procedure described in [22] is utilized. According to this procedure, K_{ij} component of the permeability tensor is defined as:

$$K_{ij} = \frac{\nu U_i}{F_j} \tag{11}$$

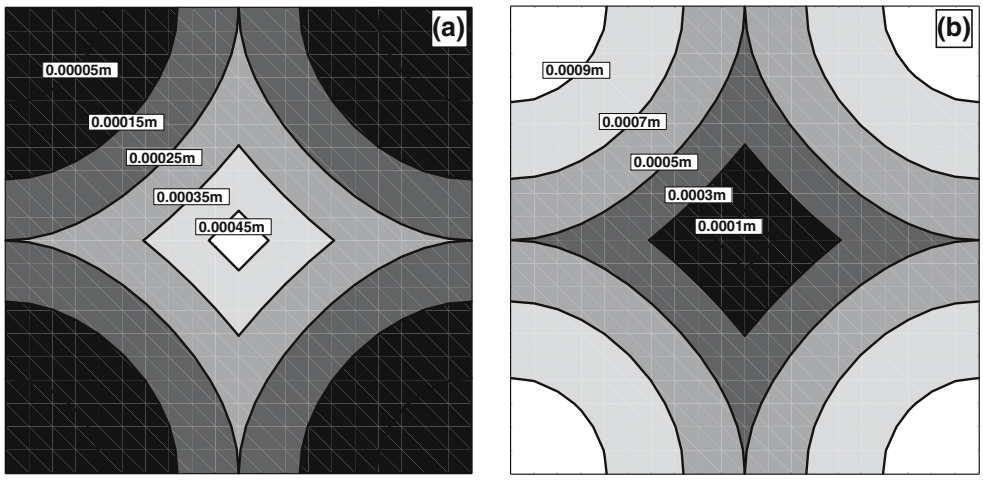

Fig. 8 (**a**) Resin channels height and (**b**) fabric thickness fields in an un-sheared one-layer orthogonal plain-weave fabric preform

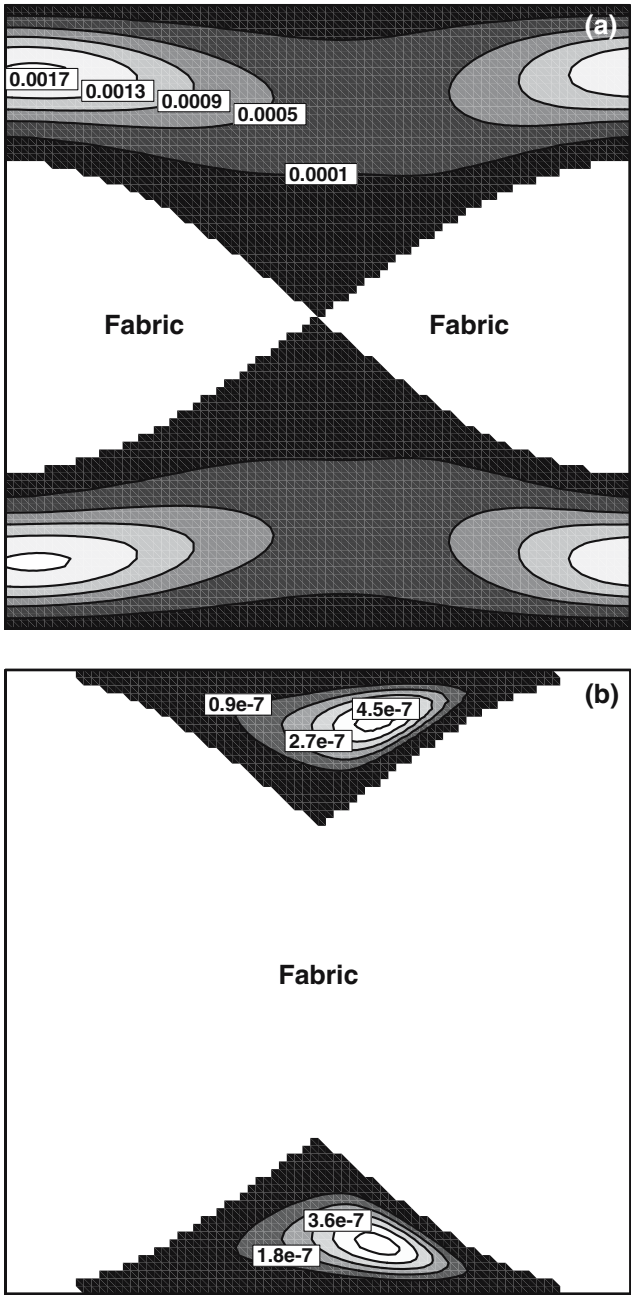

Fig. 9 The distribution of the x-component of the resin velocity in an un-sheared one-layer orthogonal plain-weave fabric preform within (**a**) $y = 0$ and (**b**) $y = L/2$ planes

where U_i is the i-component of the superficial average velocity and F_j the j-component of the body force. In other words, components of the permeability tensor are computed using the imposed pressure gradient across the computational cell in a given direction and the corresponding resulting average resin velocity. The knowledge of spatial variation of the fluid pressure is not required and is not calculated.

It should be noted that since the present analysis considers solely the macro-scale fluid flow between the fabric layers and the mold walls and not the micro-scale fluid flow between the fibers within the fabric, the effects of capillarity/surface tension are deemed secondary.

To determine the effect of the number of fabric layers on the effective permeability, the model developed in the previous section is used for the cases of 1-, 2-, 3-, 5-, 10- and 20-layer in-phase orthogonal balanced plain-weave fabric preforms in the absence of layer nesting. The results of this calculation are presented in Fig. 10. These results show that as the number of layers increases, the permeability rises but at an ever decreasing rate so that in fabric preforms with 10 or more layers, the effect of the number of layers on permeability becomes insignificant. This finding can be easily rationalized by recognizing that as the number of layers in the fabric increases, the effect of the bottom and the top resin channels which are more restrictive to the fluid flow (and thus reduce effective preform permeability) decreases. Also shown in Fig. 10 are the results of our recent calculations based on the use of a lubrication flow model [7]. Since the two sets of the results are in a very good agreement, the resin flow through the fiber preform (neglected in the present work and considered in [7]), appears to make a minor contribution to the fabric preform permeability.

Effect of fabric shear on permeability

The effect of shear deformation (measured by the magnitude of the shear angle θ) on the effective permeability of single-layer plain-weave fabric preforms is displayed in Fig. 11. An example of the variation of the

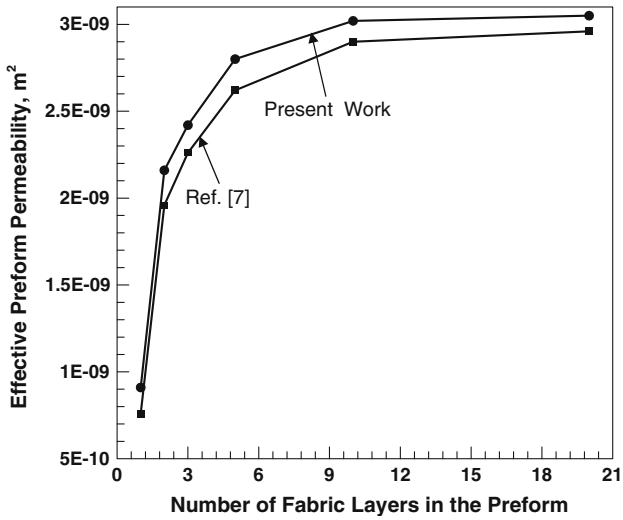

Fig. 10 The effect of the number of fabric layers on the effective permeability of an un-sheared balanced plain-weave fabric preform

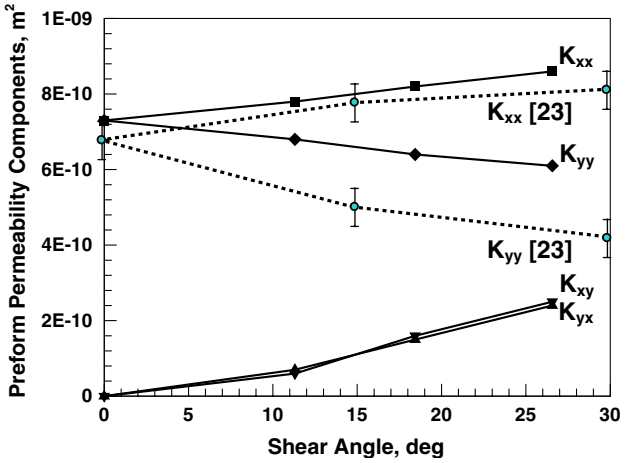

Fig. 11 The effect of shear on permeability of a single-layer balanced orthogonal plain-weave fabric preform

top- and bottom-channel heights and of the fabric thickness in the $x - y$ plane within a quarter unit cell, used as input in the present analysis, are shown in Fig. 12(a) and (b), respectively. For comparison, the experimental values of preform permeabilities obtained in [23] are also shown in Fig. 11. While the agreement between the corresponding computational and the experimental values is only fair, the effect of shear deformation on preform permeability appears to be quite well predicted by the model. In addition, the corresponding computed values of the in-plane off-diagonal (K_{xy} and K_{yx}) elements of the effective permeability are very close as required by symmetry of the orthogonal plain-weave fabric architecture.

When the fabric is sheared in the x-direction, as shown in 4(b), weft tows are rotated but remain stress free. Consequently, the dimension of the fabric-preform unit cell in the y-direction is altered causing a change in the effective fiber volume fraction in the unit cell. This change in the fiber volume fraction can have a significant effect on preform permeability at large shear angles and, hence, must be taken into account. The procedure described below is used to correct the values of permeabilities in the sheared fabrics obtained using the Lattice Boltzmann method.

To quantify the permeability correction described above, the Kozeny–Carman relation (e.g., [24]) for permeability of the porous media with a fibrous architecture is used. According to this relation, permeability of such media is given by:

$$K = \frac{r_{\mathrm{f}}^2 (1 - f_{\mathrm{f}})^3}{c f_{\mathrm{f}}^2} \tag{12}$$

where r_{f} and f_{f} are the fiber radius and the fiber volume fraction, respectively, while c is a fibrous-medium architecture-dependent constant. It should be noted that Eq. (11) is based on the assumption that no shear of the fibers accompanies fabric shear. Furthermore, it is possible to more accurately account for the change in the effective fiber volume fraction in the unit cell through a direct simulation of the fabric shear process. However, such an analysis was beyond the scope of the present work.

When the fabric preform is sheared in the x-direction by an angle θ, the fiber volume fraction in fabric tows changes as:

$$f_{\mathrm{f},\theta} = \frac{f_{\mathrm{f,o}}}{\sin(90 - \theta)} \tag{13}$$

where the angle θ is given in degrees and the subscripts o and θ are used to denote the value of a respective quantity in the un-sheared fabric and in the fabric sheared by an angle θ, respectively.

To account for a shear-induced change in the fiber volume fraction, the permeability values for sheared

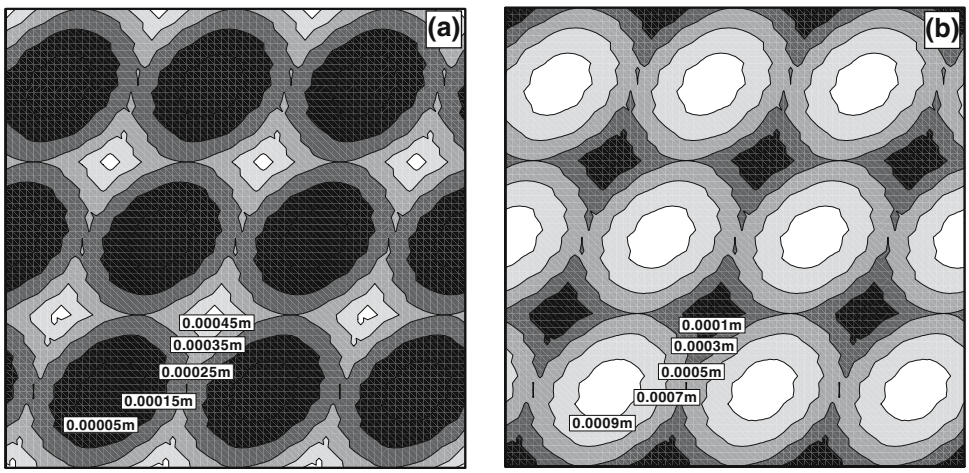

Fig. 12 (**a**) Resin channels height and (**b**) fabric thickness fields in a one-layer orthogonal plain-weave fabric preform subjected to shear in the x-direction by an angle of $\alpha = \tan^{-1}(1/3)$.

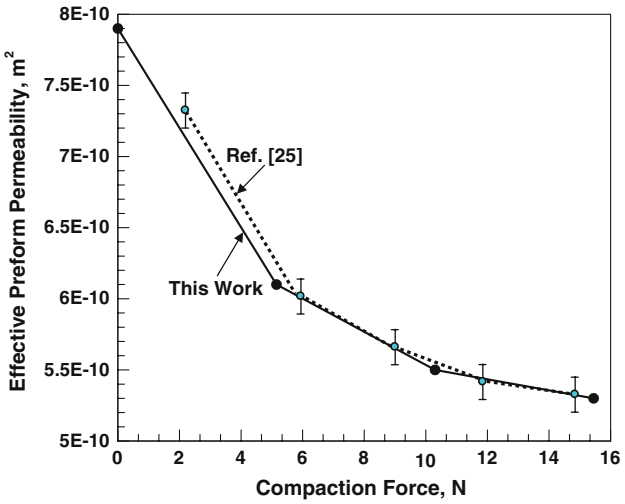

Fig. 13 Effect of compaction (represented by the magnitude of the compaction force) on permeability of a one-layer un-sheared orthogonal plain-weave fabric preform

fabric preforms obtained using the Lattice Boltzmann method are multiplied by the following correction factor:

$$K_{\text{corr}} = \frac{f_o^2(1-f_\theta)^3}{(1-f_o)^3 f_\theta^2} \tag{14}$$

It should be noted that the effect of fabric shear on permeability analyzed in the present work is fairly simplified and does not include the role of potentially important phenomena such as complex meso-scale tow deformation modes during fabric shear.

Effect of preform compaction on permeability

The effect of the compaction force applied to the upper and the lower (rigid and flat) molds on the effective permeability of a one-layer orthogonal plain-weave fabric is displayed in Fig. 13. In these calculations, the Young's modulus is assigned a value of 22 GPa and a sinusoidal distribution of the applied and the contacting pressures is assumed [19]. Since fabric compaction in the mold precedes resin infiltration, it is assumed that the fibrous structure is supported only by the solid material and not by the fluid. An example of the variation of the top- and the bottom-channel heights and of the fabric thickness in the $x-y$ plane within a quarter unit cell, used as input in the present analysis, are shown in Fig. 14(a) and (b), respectively. For comparison, the experimental results reported by Sozer et al. [25] are also shown in Fig. 13. It is seen that

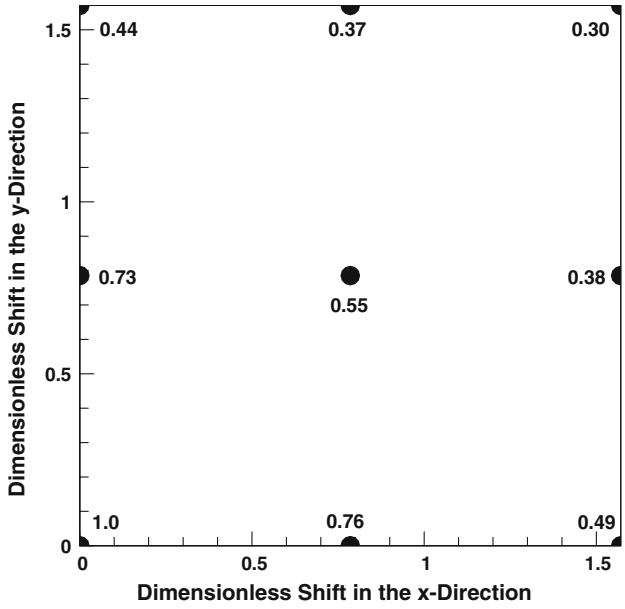

Fig. 15 The effect of nesting on the ratio of fabric permeability at the given values of layer shifts in the x- and the y-directions and fabric permeability of an un-nested in-phase laminate fabric

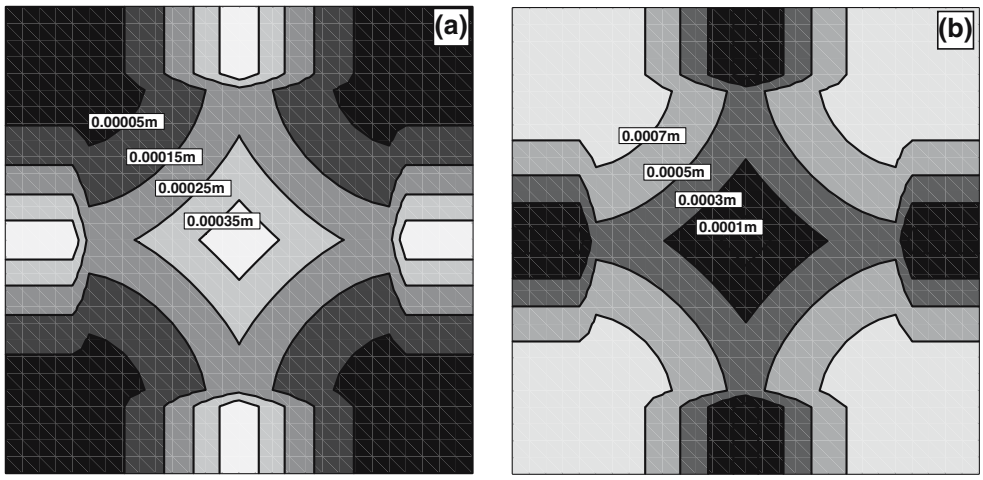

Fig. 14 (**a**) Resin channels height and (**b**) fabric thickness fields in an un-sheared one-layer orthogonal plain-weave fabric preform subject to a total compressive force of 10.3 N via rigid, flat upper and lower tool surfaces

a reasonably good agreement exists between both the magnitude of the predicted preform permeability and its change with the applied compaction force.

Effect of layer nesting

The effect of nesting (quantified by the magnitudes of the dimensionless layer shifts in the x- and the y-directions, ϕ_x and ϕ_y, respectively, in a two-layer orthogonal plain-weave fabric is shown in Fig. 15. The values displayed in Fig. 15 pertain to the ratio of fabric permeability at the given values of ϕ_x and ϕ_y and fabric permeability at $\phi_x = \phi_y = 0$. As expected, fabric nesting gives rise to the reduction in fabric permeability. Furthermore, for the case of a out-of-phase laminate fabric ($\phi_x = \phi_y = \pm \pi/2$), fabric permeability is only about 30% of its value in the in-phase laminate fabric. This finding is in excellent agreement with its experimental counterpart reported by Sozer et al. [25].

Conclusions

Based on the results obtained in the present work, the following main conclusions can be drawn:

1. Effective permeability of the orthogonal plain-weave fabric preforms can be determined computationally using the Lattice Boltzmann method for the analysis of resin flow through tool-surface/fabric-tow and tow/tow channels.
2. The computational approach presented in this work enables assessment of the contribution that various phenomena such as the mold walls, fabric shearing, interlayer shifting and restacking as well as fabric compaction due to the infiltration pressure make to orthogonal plain-weave fabric-preform permeability.
3. While no comprehensive set of experimental data is available to fully test validity of the present model, the agreement of the model predictions with selected experimental results can be generally qualified as reasonable.

Acknowledgements The material presented in this paper is based on work supported by the U.S. Army Grant Number DAAD19-01-1-0661. The authors are indebted to Drs. Walter Roy, Fred Stanton, William DeRosset and Dennis Helfritch of ARL for the support and a continuing interest in the present work. The authors also acknowledge the support of the Office of High Performance Computing Facilities at Clemson University.

References

1. Lee LJ (1997) In: Gutowski TG (eds) Advanced composites manufacturing. John Wiley & Sons, New York, pp. 393–456
2. Lam RC, Kardos JL (1988) In: Proc Third Tech Conf. American Society for Composites
3. Gutowski TG (1985) in SAMPE Quart 4
4. Gebart BR (1992) J Compos Mater 26:1100
5. Ranganathan S, Phelan F, Advani SG (1996) Polym Compos 17:222
6. Ranganathan S, Wise GM, Phelan FR, Parnas RS, Advani SG (1994) A numerical and experimental study of the permeability of fiber preforms. In: Proc Tenth ASM/ESD Advanced Composites Conf, Oct
7. Grujicic M, Chittajallu KM, Walsh S, Grujicic M (2003) Effect of shear, compaction and nesting on permeability of the orthogonal plain-weave fabric preforms. Applied Surface Science, submitted for publication, Oct
8. Martys N, Chen H (1996) Phys Rev 53:743
9. Kandhai D, Vidal DJE, Hoekstra AG, Hoefsloot H, Iedema P, Sloot PMA (1998) Intl J Modern Phys C 9:1123
10. Spaid MAA, Phelan FR (1997) Phys Fluids 9:2468
11. Chen S, Doolen GD (1998) Annu Rev Fluid Mech 30:329
12. Dungan FD, Senoguz MT, Sastry AM, Faillaci DA (2001) J Compos Mater 35:1250
13. Ito M, Chou TW (1998) J Compos Mater 32:2
14. Pearce N, Summerscales J (1995) Compos Manuf 6:15
15. Saunders RA, Lekakou C, Bader MG (1998) Compos Part A 29A:443
16. Hu J, Newton A (1997) J Text Inst Part I 88:242
17. Chen B, Chou TW (1999) Compos Sci Technol 59:1519
18. Chen B, Chou TW (2000) Compos Sci Technol 60:2223
19. Chen B, Lang EJ, Chou TW (2001) Mater Sci Eng A317:188
20. Bhatnager PL, Gross EP, Krook M (1954) Phys Rev 94:511
21. Chen H, Chen S, Mathaeus WH (1992) Phys Rev A 45:5339
22. Stockman HW (1999) Sandai Report, Sand99-0162
23. Dungan FD, Senoguz MT, Sastry AM, Faillaci DA (2001) J Compos Mater 35:1250
24. Dungan FD, Senoguz MT, Sastry AM, Faillaci DA (1999) J Reinforced Plastics Compos 18:472
25. Sozer EM, Chen B, Graham PJ, Bickerton S, Chou TW, Advani SG (1999) Proceedings of the fifth international conference on flow processes in composite materials, Plymouth, UK, 12–14 July, pp 25–36